Supporting Information

Vertically Oriented Cobalt Selenide/NiFe Layered-Double-Hydroxide Nanosheets Supported on Exfoliated Graphene Foil: An Efficient 3D Electrode for Overall Water Splitting

Yang Hou, Martin R. Lohe, Jian Zhang, Shaohua Liu, Xiaodong Zhuang, and Xinliang Feng*

Department of Chemistry and Food Chemistry, and Center for Advancing Electronics Dresden, Technische Universitaet Dresden, 01062 Dresden, Germany

E-mail: xinliang.feng@tu-dresden.de

Experimental Section

Preparation of Graphite Foil (5 s):

Graphite foil (5 s) was fabricated by anodization of graphite foil in 0.1 M $(NH_4)_2SO_4$ electrolyte with a Pt counter electrode under 10 V for 5 s.

Preparation of EG:

EG was fabricated by anodization of graphite foil in 0.1 M $(NH_4)_2SO_4$ electrolyte with a Pt counter electrode under 10 V for 15 s.[1]

Preparation of EG/$Co_{0.85}Se$:

In a typical experiment, 0.146 g $Co(NO_3)_2 \bullet 6H_2O$ and 0.087 g Na_2SeO_3 were dispersed in 18.4 mL deionized water and sonicated for about 5 min under ambient conditions. After that, 1.6 mL hydrazine hydrate was added into the above suspension. After vigorous mechanical stirring for about 10 min to dissolve completely, the resultant solution was transferred into a 25 mL of Teflon autoclave. As-prepared EG foil was then put into the solution and leaned against the autoclave, which was further sealed and heated at 140 ^{o}C for 24 h. The obtained EG/$Co_{0.85}Se$ sample was collected and rinsed with ethanol and distilled water in turn several times, and then dried under a vacuum at 60 ^{o}C for 4 h. The loading amount of EG/$Co_{0.85}Se$ on graphite foil was ~

2.7 mg cm^{-2}.

Preparation of EG/$Co_{0.85}$Se/NiFe-LDH:

To obtain the product of EG/$Co_{0.85}$Se/NiFe-LDH, the prepared EG/$Co_{0.85}$Se was immersed in a 25 mL Teflon autoclave with a homogeneous solution of $Ni(NO_3)_2$●$6H_2O$ (0.093 g), $Fe(NO_3)_3$●$9H_2O$ (0.033 g), urea (0.043 g), trisodium citrate (0.01 g), and H_2O (20 mL). The Teflon autoclave was subsequently sealed and maintained at 150 °C for 48 h to allow the growth of NiFe-LDH nanosheets on EG/$Co_{0.85}$Se foil to form the EG/$Co_{0.85}$Se/NiFe-LDH hybrid. The loading amount of EG/$Co_{0.85}$Se/NiFe-LDH on graphite foil was ~ 4.0 mg cm^{-2} (The mass loading of 4 mg cm^{-2} refers to whole EG/$Co_{0.85}$Se/NiFe-LDH hybrid except the graphite foil substrate).

Preparation of EG/NiFe-LDH:

The EG foil was immersed in a 25 mL Teflon autoclave with a homogeneous solution of $Ni(NO_3)_2$●$6H_2O$ (0.093 g), $Fe(NO_3)_3$●$9H_2O$ (0.033 g), urea (0.043 g), trisodium citrate (0.01 g), and H_2O (20 mL). The Teflon autoclave was subsequently sealed and maintained at 150 °C for 48 h to allow the growth of NiFe-LDH nanosheets on EG foil to form the EG/NiFe-LDH hybrid. The loading amount of EG/NiFe-LDH on graphite foil was ~ 3.3 mg cm^{-2}.

Preparation of underloaded-NiFe-LDH/$Co_{0.85}$Se/EG:

The EG/$Co_{0.85}$Se/NiFe-LDH sample obtained by halving NiFe-LDH precursor feed is defined as underloaded-NiFe-LDH/$Co_{0.85}$Se/EG. In a typical experiment, the obtain EG/$Co_{0.85}$Se was immersed in a 25 mL Teflon autoclave with a homogeneous solution of $Ni(NO_3)_2$●$6H_2O$ (0.047 g), $Fe(NO_3)_3$●$9H_2O$ (0.017 g), urea (0.022 g), trisodium citrate (0.005 g), and H_2O (20 mL). The Teflon autoclave was subsequently sealed and maintained at 150 °C for 48 h to allow the growth of a small number of NiFe-LDH nanosheets on EG foil to form the underloaded-NiFe-LDH/$Co_{0.85}$Se/EG.

Preparation of overloaded-NiFe-LDH/$Co_{0.85}$Se/EG:

The EG/$Co_{0.85}$Se/NiFe-LDH sample obtained by doubling NiFe-LDH precursor feed is defined as overloaded-NiFe-LDH/$Co_{0.85}$Se/EG. In a typical experiment, the obtained EG/$Co_{0.85}$Se was immersed in a 25 mL Teflon autoclave with a

homogeneous solution of $Ni(NO_3)_2 \bullet 6H_2O$ (0.186 g), $Fe(NO_3)_3 \bullet 9H_2O$ (0.066 g), urea (0.086 g), trisodium citrate (0.02 g), and H_2O (20 mL). The Teflon autoclave was subsequently sealed and maintained at 150 °C for 48 h to allow the growth of a large number of NiFe-LDH nanosheets on EG foil to form the overloaded-NiFe-LDH/$Co_{0.85}Se$/EG.

Preparation of Active Carbon Paper (ACP):

In a typical synthesis, CP was cleaned with ethanol and deionized water, respectively, and then treated in concentrate HNO_3 (6.0 M) at 100 °C for 5 h, followed by washing with deionized water. The obtained ACP sample was dried at 120 °C for 12 h.

Preparation of ACP/$Co_{0.85}Se$:

In a typical experiment, 0.146 g $Co(NO_3)_2 \bullet 6H_2O$ and 0.087 g Na_2SeO_3 were dispersed in 18.4 mL deionized water and sonicated for about 5 min under ambient conditions. After that, 1.6 mL hydrazine hydrate was added into the above suspension. After vigorous mechanical stirring for about 10 min to dissolve completely, the resultant solution was transferred into a 25 mL of Teflon autoclave. As-prepared ACP foil was then put into the solution and leaned against the autoclave, which was further sealed and heated at 140 ^{o}C for 24 h. The obtained ACP/$Co_{0.85}Se$ sample was collected and rinsed with ethanol and distilled water in turn for several times, and then dried under a vacuum at 60 ^{o}C for 4 h.

Preparation of Physical Mixture of EG, $Co_{0.85}Se$, and NiFe-LDH:

EG power was obtained by scratching down the EG from graphite foil. Then, the EG, $Co_{0.85}Se$, and NiFe-LDH powers were ground together to form the physical mixture of EG, $Co_{0.85}Se$, and NiFe-LDH as a reference. The mass ratio of NiFe-LDH: $Co_{0.85}Se$: EG in the physical mixture is the same with that of the EG/$Co_{0.85}Se$/NiFe-LDH hybrid. The obtained product was ultrasonically dispersed in the mixture of Nafion solution and ethanol, and then transferred onto the glassy carbon electrode via a controlled drop casting method to afford a loading amount of ~ 4.0 mg cm^{-2}. Physical mixture of EG and $Co_{0.85}Se$ was synthesized by the same procedure without NiFe-LDH.

Preparation of EG after Annealing in Ar

EG foil was further reduced by heat treatment in a tube furnace at 700 °C under Ar

flowing for 2 h.

Characterization:

The morphology, microstructure, and element composition of the products were examined by the field emission scanning electron microscope (FESEM, Carl Zeiss NVision 40) equipped with an energy-dispersive X-ray spectroscopy (EDX) analyzer and transmission electron microscope (TEM, Carl Zeiss, Libra 120 and Libra 200). Powder X-ray diffraction (XRD) measurement was performed on SIEMENS D5000 diffractometer. The contact angle was measured on a ‘‘DSA-10’’ Kruss contact angle goniometer. X-ray photoelectron spectroscopy (XPS) analysis was carried out on an a AXIS Ultra DLD system Kratos using Al as the excitation source. Raman spectra were recorded using an NTEGRA Spectra system (NT-MDT). Fourier transform infrared spectra (FTIR) were measured on a BRUKER TENSOR II spectrometer. N_2 adsorption isotherms were collected on a Quadrasorb Adsorption Instrument at the liquid nitrogen temperature. The inductively coupled plasma–optic emission spectrometry (ICP-OES) tests were performed using a Perkin Elmer Optima 7000DV. The electrical resistivity of as-prepared electrodes was measured using a four-point probe system (Jandel Model RM3000 system). The synthesized EG-based nanoarray electrodes were carefully scraped off from graphite foil and used for TEM, XRD, FTIR, EDX, ICP-OES, and N_2 adsorption measurements. For FESEM, XPS, contact angle, and Raman, the nanoarrays grown on graphite foil were measured directly.

Electrochemical measurements

Oxygen evolution reaction (OER) and hydrogen evolving reaction (HER)

All electrochemical measurements were conducted on an electrochemical analyzer (CHI 760 E, CH Instruments, USA). A conventional three-electrode cell was used, including as-prepared EG/$Co_{0.85}$Se/NiFe-LDH foil as the working electrode, a Ag/AgCl electrode as the reference electrode, and Pt wire as the counter electrode. The reference was calibrated against and converted to reversible hydrogen electrode (RHE) according to the Nernst equation ($E_{RHE} = E_{Ag/Ag/Cl} + 0.059 \times pH + 0.197$). Linear sweep voltammetry (LSV) was carried out in 1.0 M KOH electrolyte with a scan rate of 1 mV s^{-1} to obtain the polarization curves. The long-term durability test

was performed using chronopotentiometric and chronoamperometric measurements. Before recording, the electrodes were cycled until a stable cyclic voltammetry (CV) curve was obtained. The electrochemical impedance spectroscopy (EIS) was carried out in the range from 100 K to 0.01 Hz with an AC amplitude of 10 mV. Unless otherwise noted, all polarization curves were iR corrected.

Overall water splitting

Overall water splitting studies were performed using a CHI 760 E potentiostat (CH Instruments, USA) in a two-electrode system with one EG/$Co_{0.85}$Se/NiFe-LDH electrode acting as the positive electrode for OER and the other EG/$Co_{0.85}$Se/NiFe-LDH electrode acting as the negative electrode for OER. Prior to measurement, the resistance test was made and the iR compensation was applied, which is similar with OER or HER measurements. The electrocatalytic activity of EG/$Co_{0.85}$Se/NiFe-LDH electrode towards the overall water splitting was examined by polarization curves using linear sweep voltammetry (LSV) in 1.0 M KOH with scan rate of 1 mV s^{-1}. For comparison, 20 mg of Pt/C (or Ir/C) was dispersed in 0.2 mL Nafion solution (0.5 wt.%) and 0.8 mL ethanol in an ultrasonic bath. The dispersion was then transferred onto the graphite foil via a controlled drop casting method. The mass loading of the Pt/C (or Ir/C) was controlled to obtain a loading amount of 4.0 mg cm^{-2}, the same as that of EG/$Co_{0.85}$Se/NiFe-LDH on graphite foil.

Determination of mass activity

The values of mass activity (mA mg^{-1}) were calculated from the catalyst loading m (mg cm^{-2}) and the measured current density J (mA cm^{-2}) at 1.52 V.

$$\text{Mass activity} = J/m$$

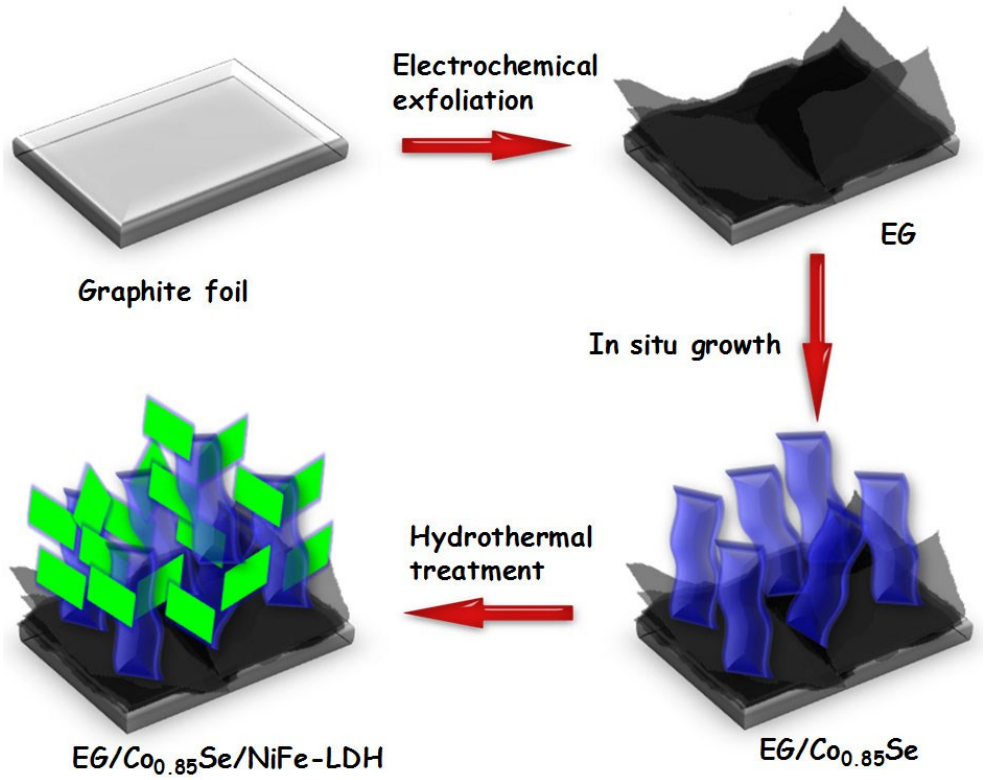

Figure S1. Schematic illustration for the synthesis process of EG/$Co_{0.85}$Se/NiFe-LDH.

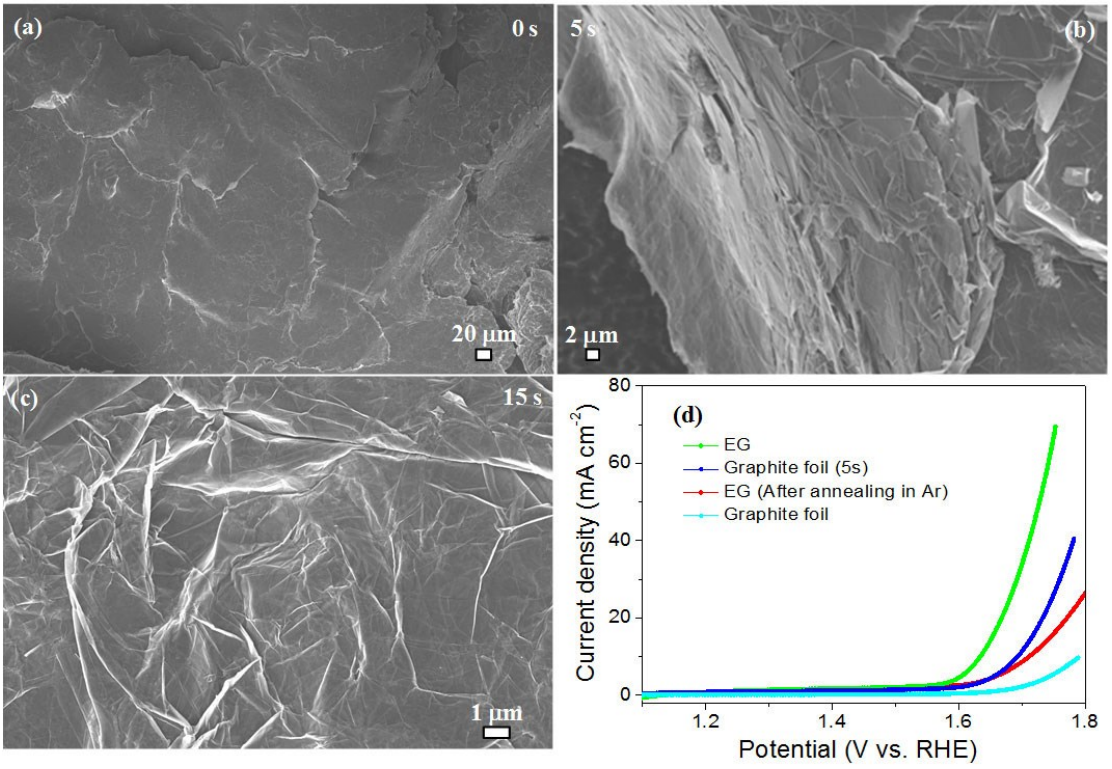

Figure S2. FESEM images of (a) graphite foil, (b) graphite foil (5s), and (c) EG. (d) polarization curves of graphite foil, graphite foil (5s), EG, and EG after annealing in

Ar in 1.0 M KOH solution.

The exfoliation time could significantly influence the activities of EG for OER. It was found that the OER performance enhanced along with the increase of exfoliation time of graphite foil (0-15 s). Such increasing OER activity can be ascribed to the increase in the number of accessible reactive sites (Figure S2a-S2c) and its defect structure (Figure S16-S17). The C atoms adjacent to the substituted oxygen groups may function as active sites by redistributing their charge and spin density for water dissociation[2] due to the high electro-negativity of O species.[3] In order to support this demonstration, we investigated the effect of different amount of relative oxygen groups in EG for OER performance. The EG with a high amount of oxygen content (8.6 atom%, from XPS results) exhibited a much higher OER activity than those of EG after annealing in Ar (the oxygen content of 3.5 atom%) and graphite foil (5s, the oxygen content of 2.5 atom%). The results indicate that the substituted oxygen groups in EG play an important role in the OER processes.

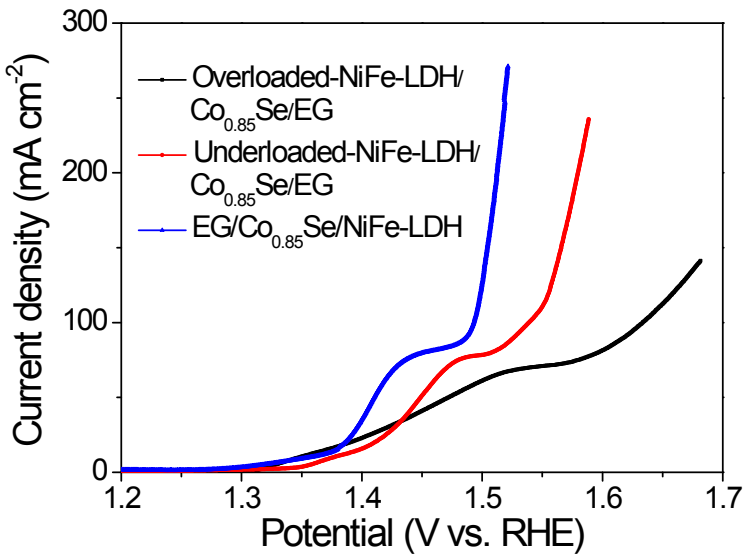

Figure S3. Polarization curves of EG/$Co_{0.85}$Se/NiFe-LDH, underloaded-NiFe-LDH/$Co_{0.85}$Se/EG, and overloaded-NiFe-LDH/$Co_{0.85}$Se/EG in 1.0 M KOH solution.

As shown in Figure S3, two relevant samples, that are, underloaded-NiFe-

LDH/$Co_{0.85}Se$/EG and overloaded-NiFe-LDH/$Co_{0.85}Se$/EG (For details see experimental section), were prepared by halving and doubling the NiFe-LDH precursor feed, respectively, and their properties were examined. Both of them exhibited higher onset potentials, lower cathodic current densities, and larger overpotentials at 150 mA cm^{-2} than that of EG/$Co_{0.85}Se$/NiFe-LDH. The results indicate that the NiFe-LDH incorporation with a small amount could partially improve the OER activity of the EG/$Co_{0.85}Se$ by forming synergistic NiFe-LDH. However, the overloaded-NiFe-LDH will increase the charge-transfer resistance and depress active sites exposure on the surface of EG/$Co_{0.85}Se$, leading to lower OER activity.

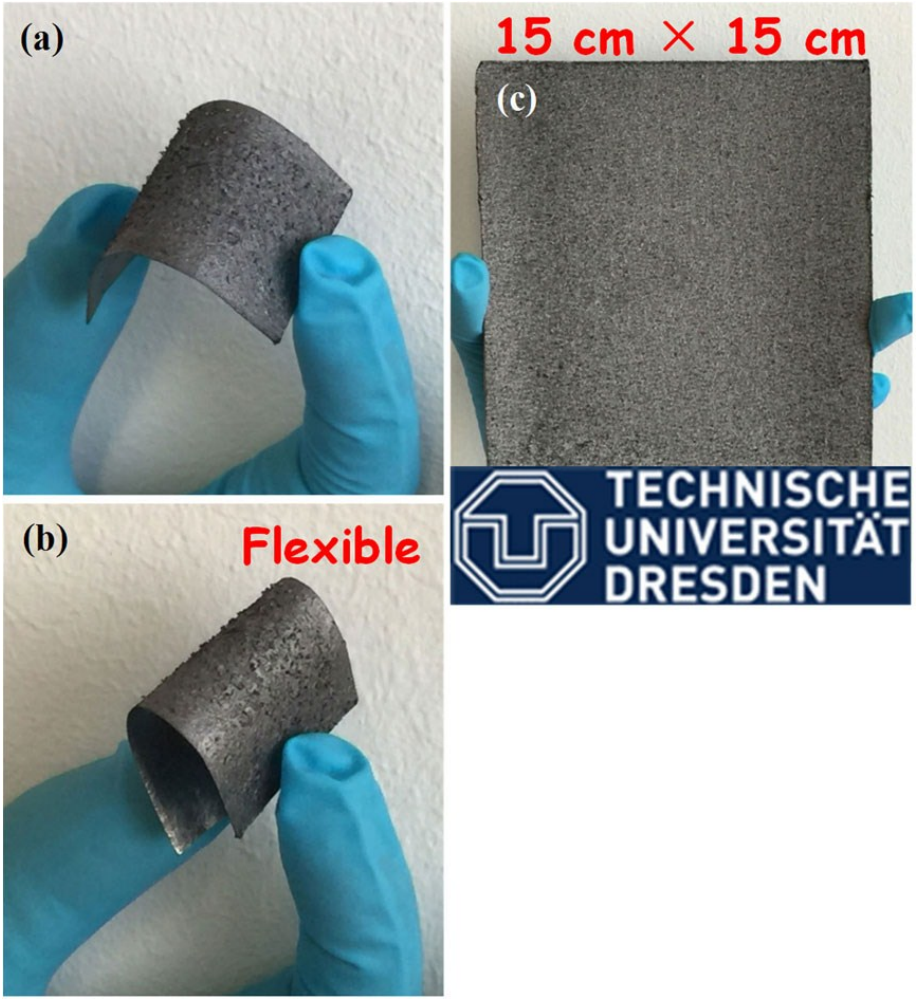

Figure S4. Photographs of the flexible EG electrodes (a-b) and the EG electrode with a large size of 15 cm × 15 cm (c).

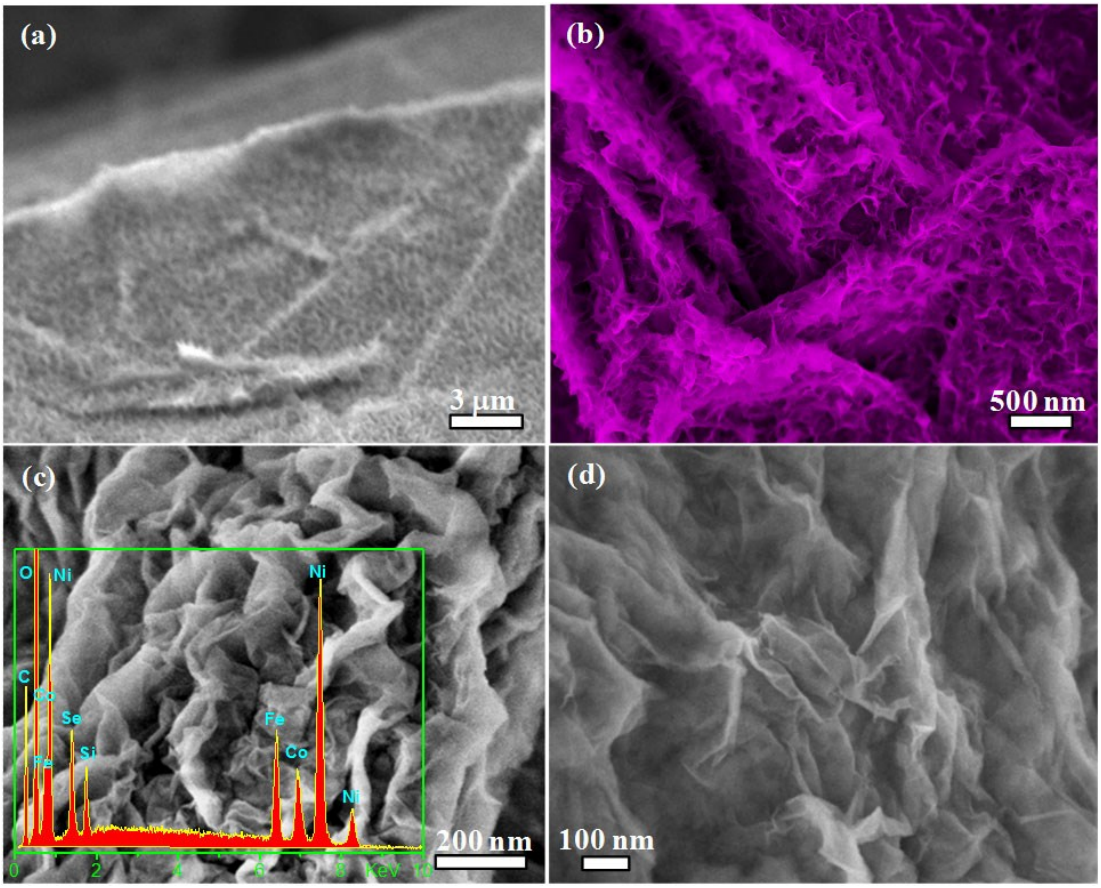

Figure S5. (a) FESEM image of EG/$Co_{0.85}Se$ and (b-d) FESEM images of EG/$Co_{0.85}Se$/NiFe-LDH with different magnification. Inset in (c) is the corresponding EDX spectrum.

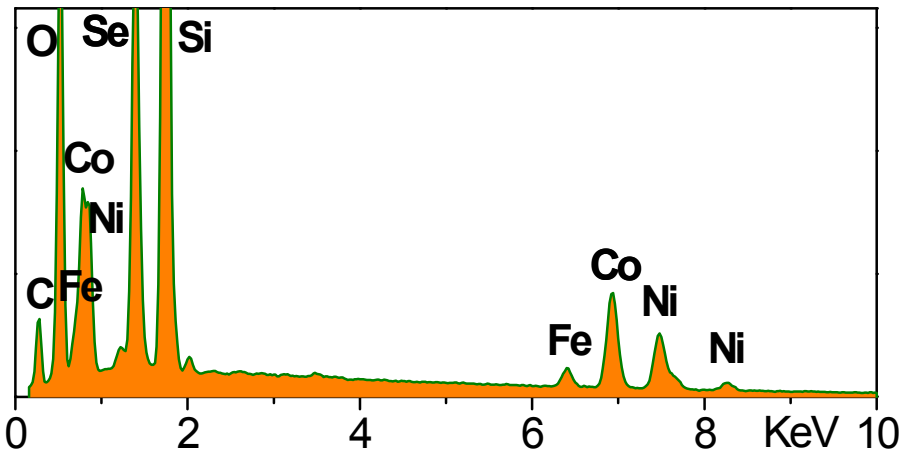

Figure S6. EDX spectrum of EG/$Co_{0.85}Se$/NiFe-LDH.

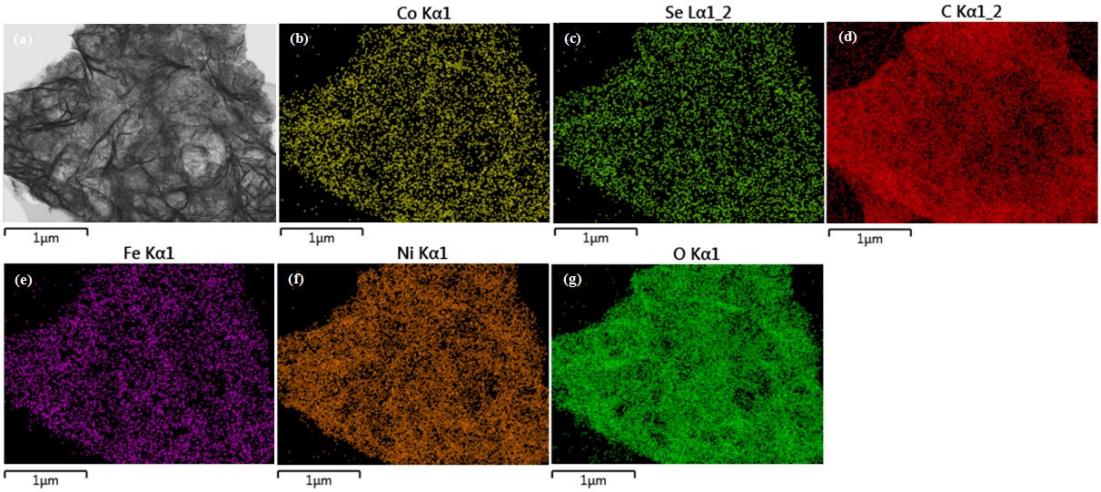

Figure S7. FESEM image (a) and corresponding elemental mappings (b-g) of EG/$Co_{0.85}$Se/NiFe-LDH.

Elemental mapping images of the EG/$Co_{0.85}$Se/NiFe-LDH hybrid disclose the well-defined spatial distribution of all elements Co, Se, Fe, Ni, O, and C in the hybrid (Figure S7)

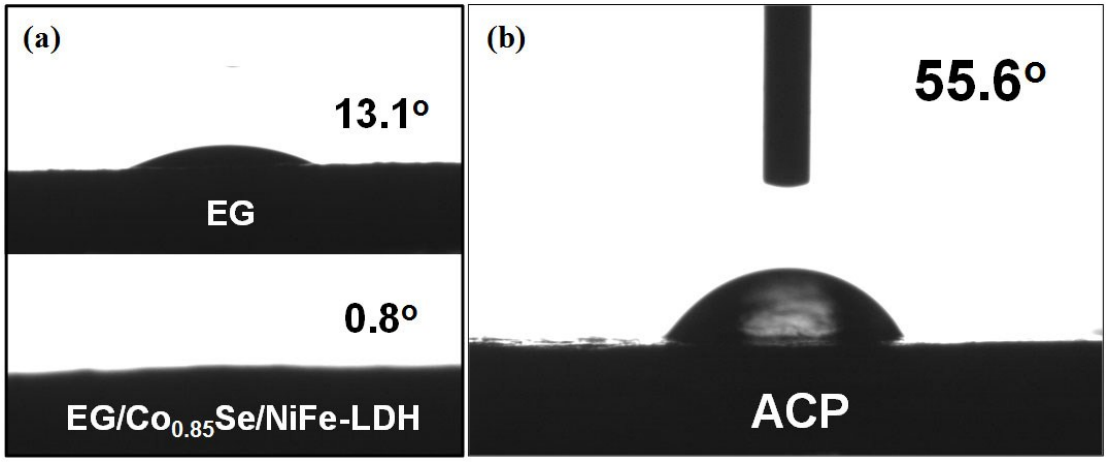

Figure S8. Contact wetting angel of EG (a), EG/$Co_{0.85}$Se/NiFe-LDH (a), and ACP (b). The EG/$Co_{0.85}$Se/NiFe-LDH is highly hydrophilic in nature with a small contact angle of ~ 0.8°, in contrast to 13.1° and 55.6° of the EG and ACP, respectively.

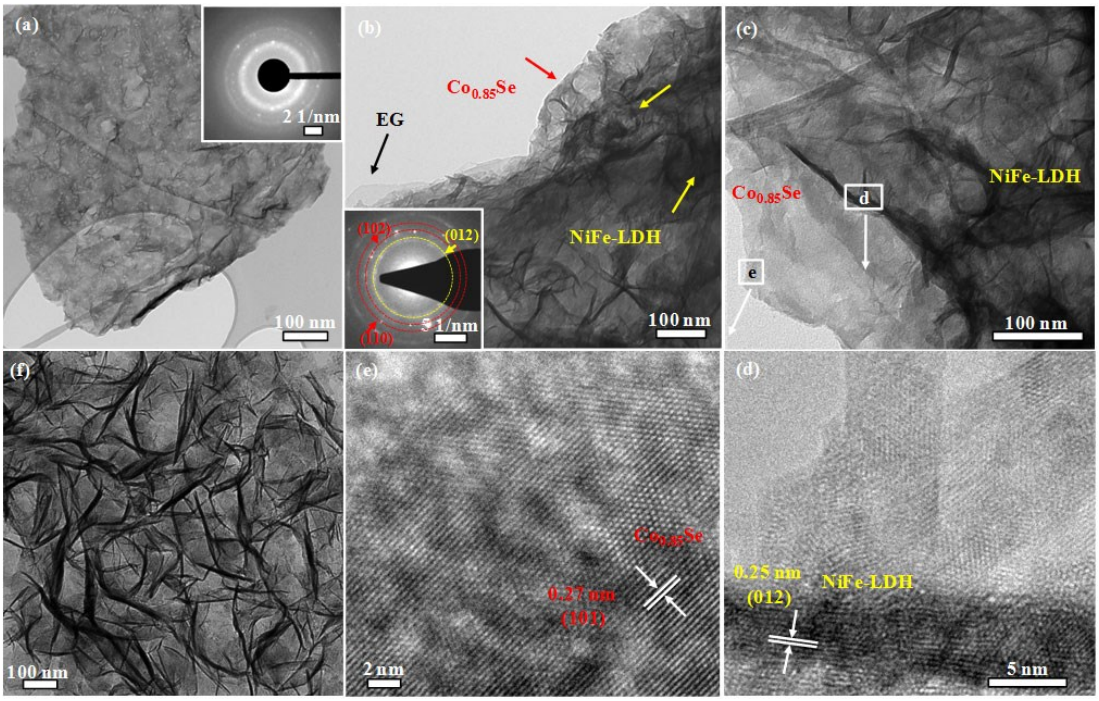

Figure S9. TEM and HRTEM images of EG/$Co_{0.85}Se$ (a), EG/$Co_{0.85}Se$/NiFe-LDH (b-e), and NiFe-LDH (f). Insets in (a-b) are the corresponding SAED patterns.[4] (d and e) show HRTEM images of EG/$Co_{0.85}Se$/NiFe-LDH from the areas labeled by the rectangular box in (c).

Further insights into the morphology of the EG/$Co_{0.85}Se$/NiFe-LDH were obtained from TEM and HRTEM images. By comparing with those of EG/$Co_{0.85}Se$ (Figure S9a) and NiFe-LDH (Figure S9f), it is obvious that the NiFe-LDH has a typical layered structure (black stripes) which grows along the surface of the EG/$Co_{0.85}Se$ (Figure S9b). The SAED pattern (inset of Figure S9b) of EG/$Co_{0.85}Se$/NiFe-LDH shows several diffraction rings made up of discrete spots, which can be indexed to the (012) plane of NiFe-LDH phase,[5] and the (102) and (110) planes of hexagonal phase $Co_{0.85}Se$.[6] The HRTEM images from the areas labeled by the rectangular frame in Figure S9c indicate that the observed lattice fringes spacing of 0.25 and 0.27 nm match well with the (012) plane of NiFe-LDH and (101) plane of $Co_{0.85}Se$,[7] respectively (Figure S9d-S9e). The above results confirm the presence and distribution of $Co_{0.85}Se$ and NiFe-LDH in the hybrid.

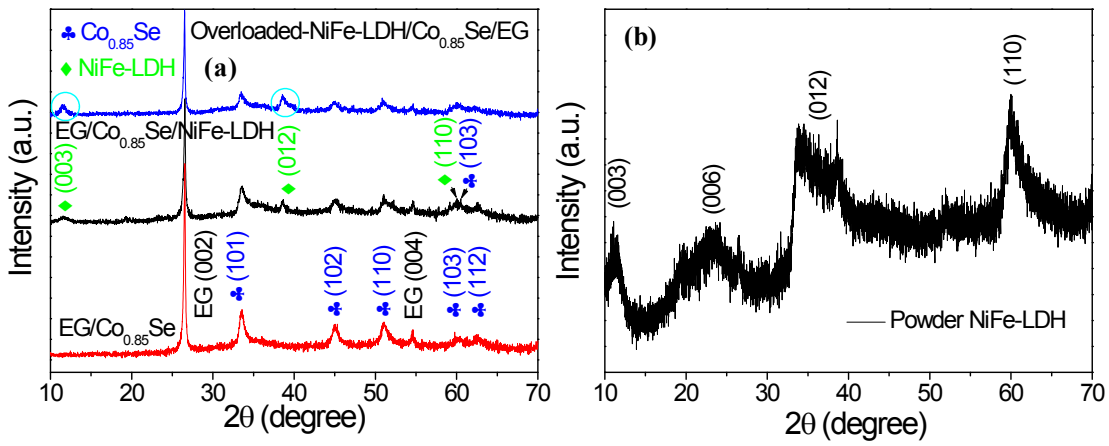

Figure S10. XRD patterns of EG/$Co_{0.85}$Se, EG/$Co_{0.85}$Se/NiFe-LDH, and overloaded-NiFe-LDH/$Co_{0.85}$Se/EG (a), and powder NiFe-LDH (b).

The crystal structure of the samples was investigated by X-ray diffraction (XRD). The EG/$Co_{0.85}$Se displays several peaks at 33.5, 45.1, 51.1, 60.4, and 62.6° corresponding to the (101), (102), (110), (103), and (112) planes, respectively, which are consistent with hexagonal phase $Co_{0.85}$Se (JCPDS 52-1008). Two sharp peaks at around 26.5 and 54.6° arise from EG indicative of the crystalline graphitic carbon. After the hydrothermal treatment, in addition to EG and $Co_{0.85}$Se, two weak peaks additionally appear at 11.7 and 38.6°, which can be indexed to the (003) and (012) planes of NiFe-LDH, respectively (Figure S10b). Besides, the EG/$Co_{0.85}$Se/NiFe-LDH shows a much strong and broad peak at 60.2° compared with EG/$Co_{0.85}$Se, may due to the overlap from two diffraction peaks of $Co_{0.85}$Se (103) and NiFe-LDH (110). In order to better reveal the existence of NiFe-LDH in the EG/$Co_{0.85}$Se/NiFe-LDH hybrid, we have doubled NiFe-LDH precursor feed and followed the same preparation process of EG/$Co_{0.85}$Se/NiFe-LDH. XRD pattern of the obtained product (overloaded-NiFe-LDH/$Co_{0.85}$Se/EG) clearly demonstrated the increase of relative intensity of (003) and (012) planes of NiFe-LDH compared with EG/$Co_{0.85}$Se/NiFe-LDH (Figure S10a), without the detection of any new diffraction peaks. This results confirm the existence of NiFe-LDH in the EG/$Co_{0.85}$Se/NiFe-LDH.

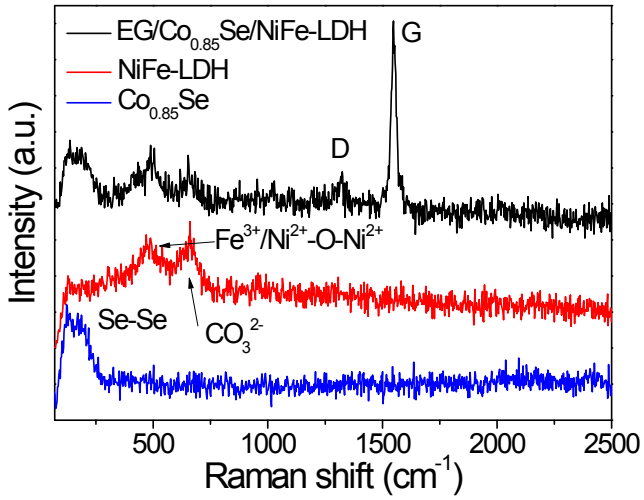

Figure S11. Raman spectra of $Co_{0.85}Se$, NiFe-LDH, and EG/$Co_{0.85}Se$/NiFe-LDH.

The insight into the structure of samples can be garnered from Raman spectroscopy (Figure S11), in which one characteristic peak for $Co_{0.85}Se$ at 172 cm^{-1} corresponding to Se-Se stretching mode,[8] two typical peaks of NiFe-LDH at 479 and 656 cm^{-1} associated with Fe^{3+}/Ni^{2+}-O-Ni^{2+} and intercalated CO_3^{2-} linkage bands,[7b, 9] respectively, and the D (1,325 cm^{-1}) and G (1,550 cm^{-1}) bands of EG can be clearly seen.[10] The intensity ratio of the D to G bands is only 0.11, which is much smaller than for traditional chemically or thermally reduced GO (> 1.0),[11] indicating a low degree of defects in the EG.

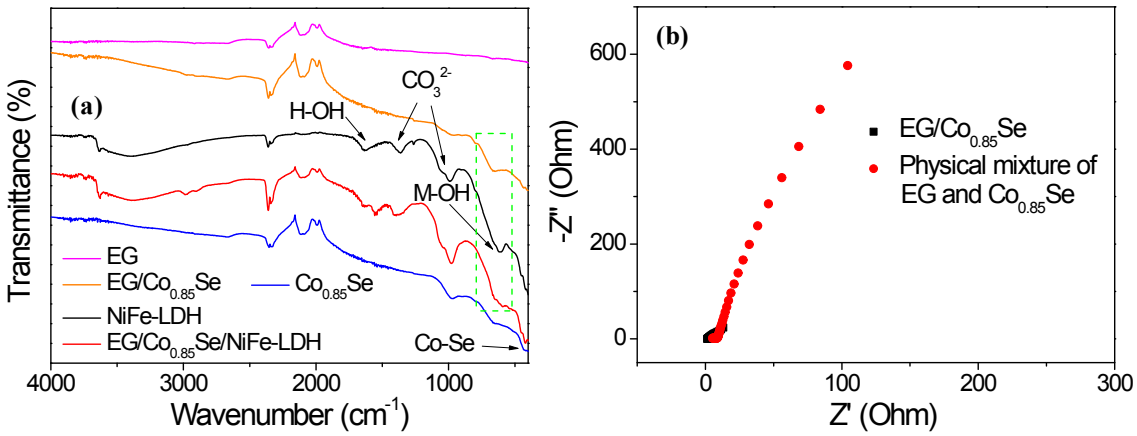

Figure S12. (a) FTIR spectra of EG, EG/$Co_{0.85}Se$, $Co_{0.85}Se$, NiFe-LDH, and EG/$Co_{0.85}Se$/NiFe-LDH. The labeled (H-OH), (CO_3^{2-}), (M-OH), and (Co-Se) are according to ***J. Mater. Sci., 2003, 38 (9): 2087-2093; J. Raman Spectrosc. 2008, 39:***

582-586 and J. Bone. Miner. Res., 2001, 16(5): 893-900. (b) EIS Nyquist plots of EG/$Co_{0.85}$Se and physical mixture of EG and $Co_{0.85}$Se.

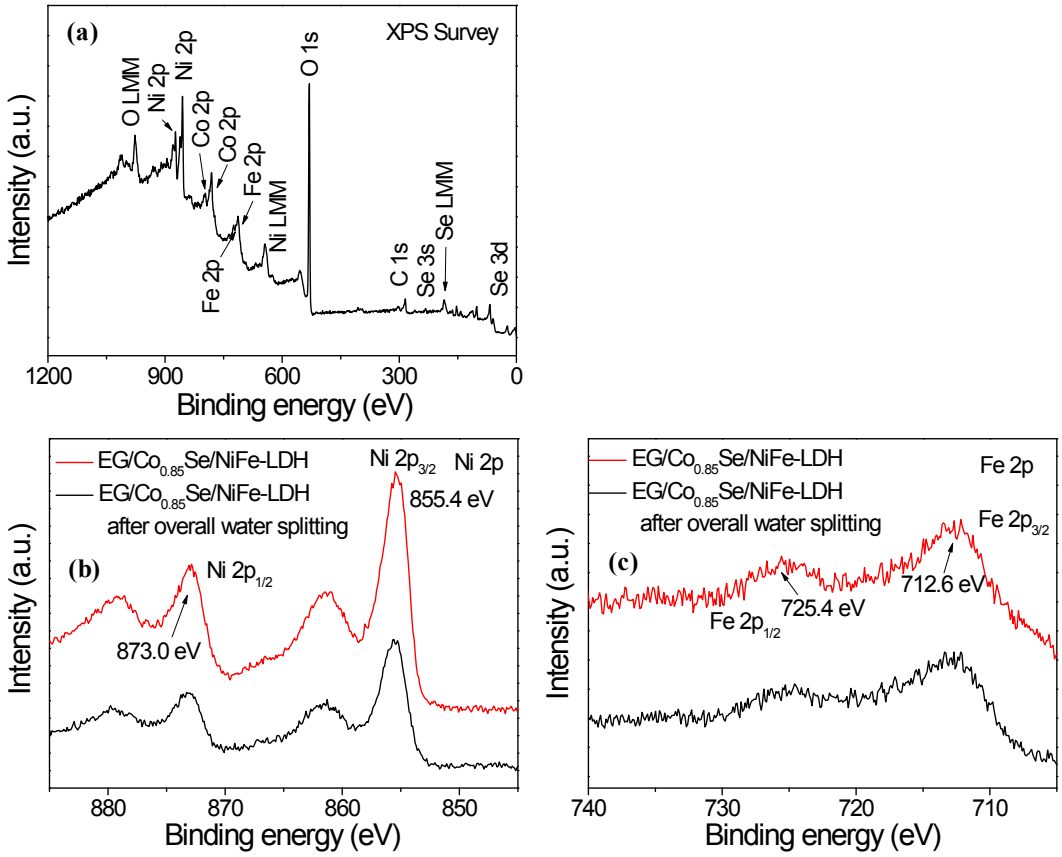

Figure S13. **XPS spectrum analysis.** (a) The survey XPS spectrum, (b) high-resolution Ni 2p XPS spectra, and (c) high-resolution Fe 2p XPS spectra of EG/$Co_{0.85}$Se/NiFe-LDH before and after overall water splitting.

The Ni $2p_{1/2}$ and Ni $2p_{3/2}$ centered at 873.0 and 855.4 eV correspond to Ni^{2+} (Figure S13b),[12] while the peaks at 712.6 and 725.4 eV can be assigned to Fe $2p_{3/2}$ and Fe $2p_{1/2}$ (Figure S13c),[13] confirming the oxidation state (+2) for Ni and (+3) for Fe in the EG/$Co_{0.85}$Se/NiFe-LDH hybrid.

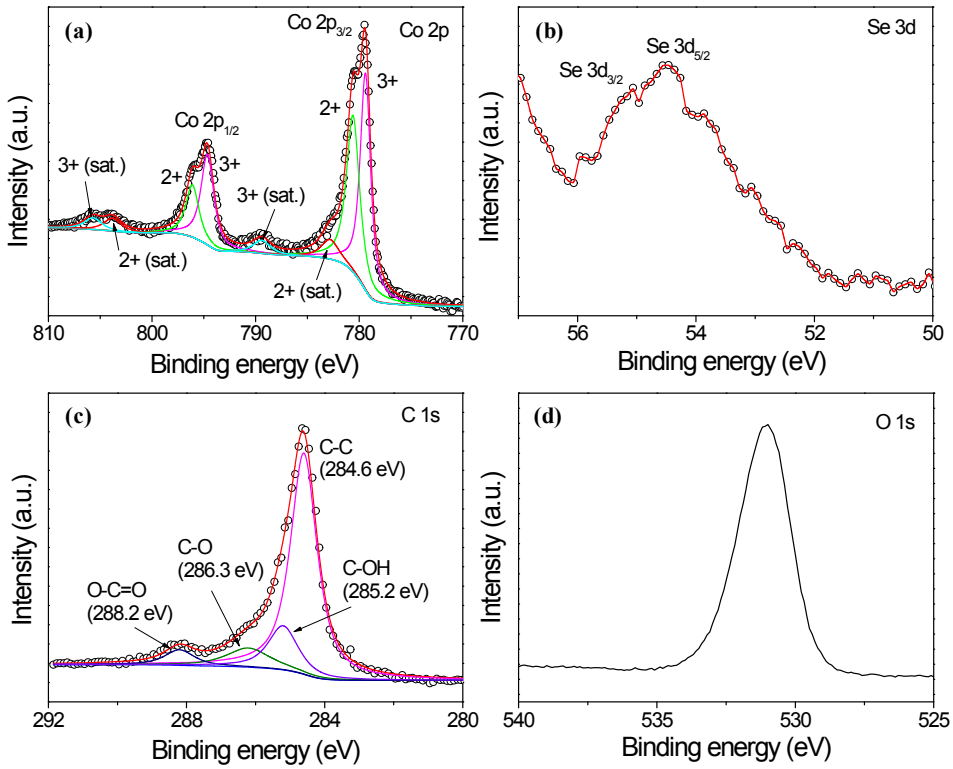

Figure S14. **XPS spectrum analysis.** (a) high-resolution Co 2p XPS spectrum, (b) high-resolution Se 3d XPS spectrum, (c) high-resolution C 1s XPS spectrum, and (d) high-resolution O 1s XPS spectrum of EG/$Co_{0.85}$Se/NiFe-LDH.

For the Co 2p and Se 3d spectra, the binding energies of Co^{2+} $2p_{3/2}$, Co^{3+} $2p_{3/2}$, Co^{2+} $2p_{1/2}$, and Co^{3+} $2p_{1/2}$ are 780.6, 779.4, 796.1, and 794.7 eV, respectively, indicating the coexistence of Co^{2+} and Co^{3+} species (Figure S14a).[4] The peaks at 55.2 and 54.5 eV were assigned to Se $3d_{3/2}$ and Se $3d_{5/2}$ (Figure S14b), respectively, which agree well with previous reports on $Co_{0.85}$Se.[14] From the C 1s spectra of EG/$Co_{0.85}$Se/NiFe-LDH (Figure S14c), four peaks centered at 284.6, 285.2, 286.3, and 288.2 eV are observed, corresponding with C–C, C–OH, C–O, and O–C=O groups, respectively.[15]

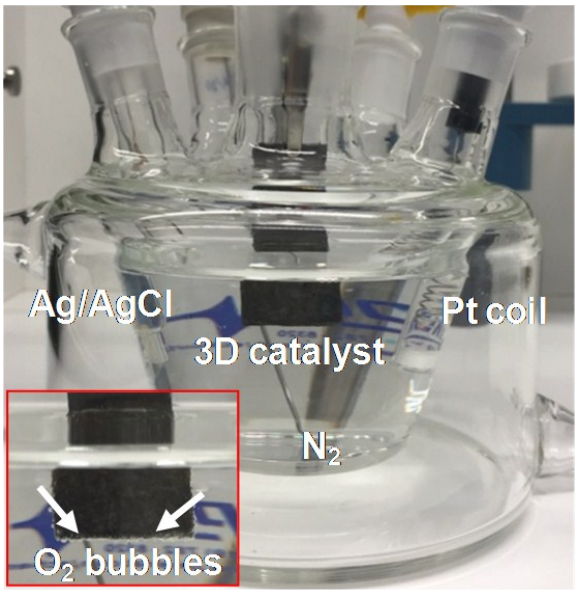

Figure S15. Optical image showing a three-electrode setup and oxygen bubbles on 3D catalyst electrode (inset) for OER.

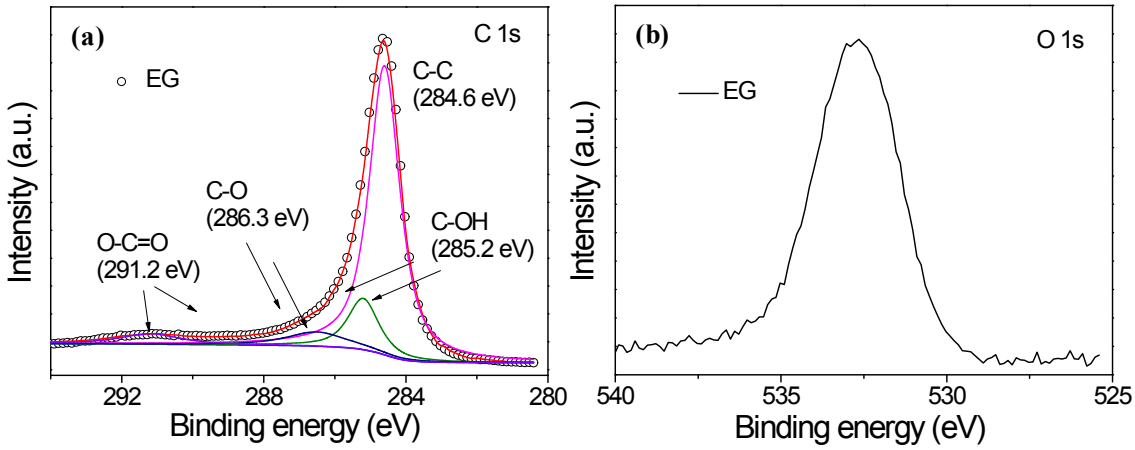

Figure S16. XPS spectrum analysis. (a) high-resolution C 1s XPS spectrum and (b) high-resolution O 1s XPS spectrum of EG.

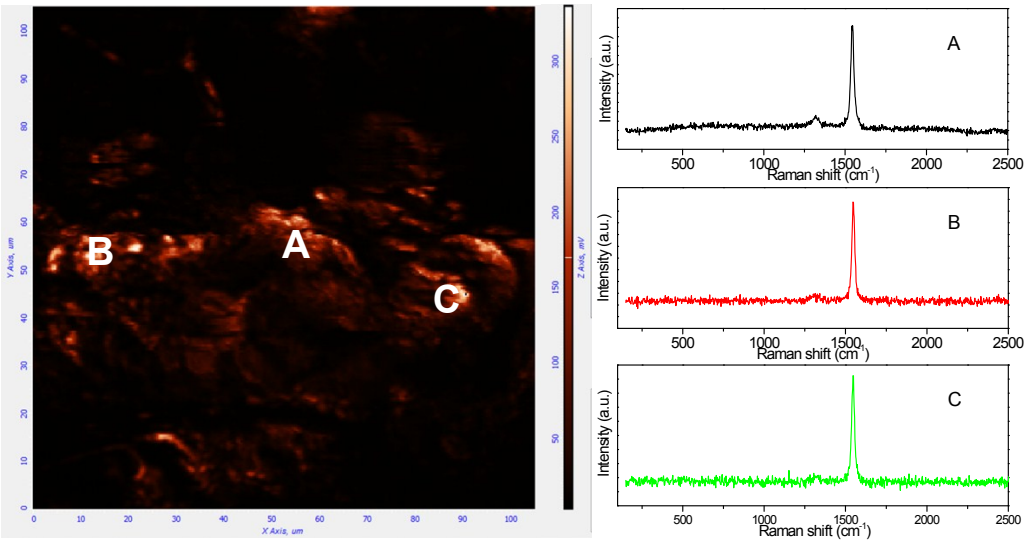

Figure S17. Raman image and the corresponding spectra of EG.

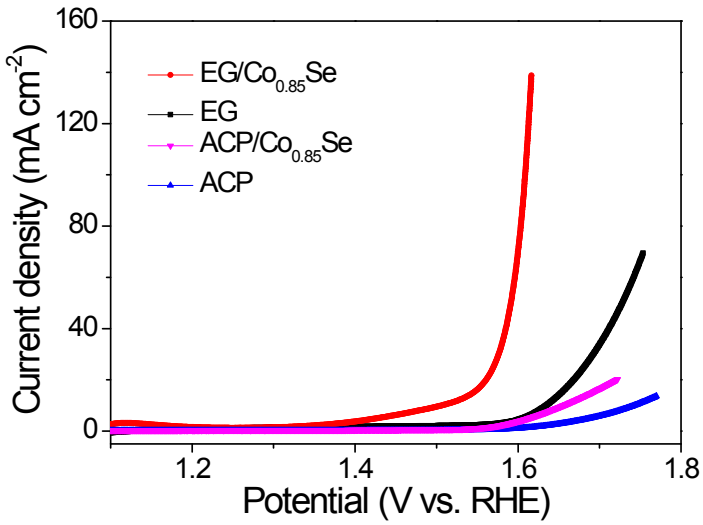

Figure S18. Polarization curves of EG, EG/$Co_{0.85}Se$, ACP, and ACP/$Co_{0.85}Se$ in 1.0 M KOH solution.

In order to further confirm that the EG played a crucial influence on the OER catalytic activity, two samples, that is, ACP (which is often used as a substrate for growth of electrocatalysts[16]) and the $Co_{0.85}Se$ nanosheets grown on ACP substrate (ACP/$Co_{0.85}Se$, Figure S18) are prepared. Both EG/$Co_{0.85}Se$ ($Co_{0.85}Se$ nanosheets grown on EG) and EG exhibited much higher OER catalytic activity than those of the materials on ACP. Besides intrinsic catalytic activity of EG, lower resistance of the EG greatly contribute to the overall catalytic activity (Figure S25). The EG/$Co_{0.85}Se$

can not only serve as an effective support for the growth of NiFe-LDH nanosheets, but also chemically couple with NiFe-LDH to promote the OER activity.

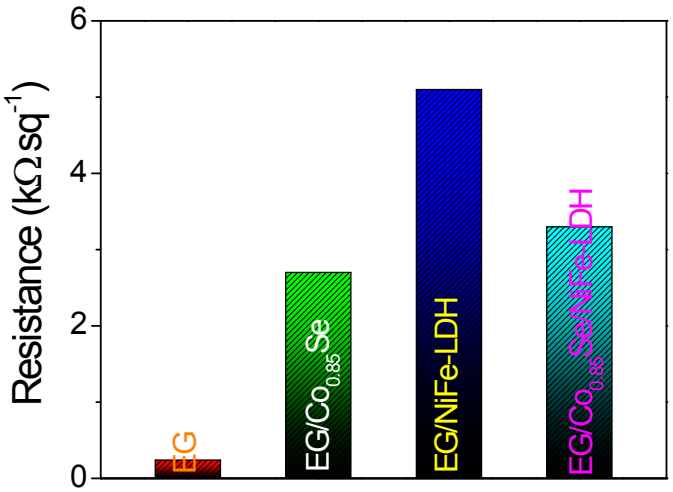

Figure S19. Resistance comparison of EG, EG/$Co_{0.85}Se$, EG/NiFe-LDH, and EG/$Co_{0.85}Se$/NiFe-LDH.

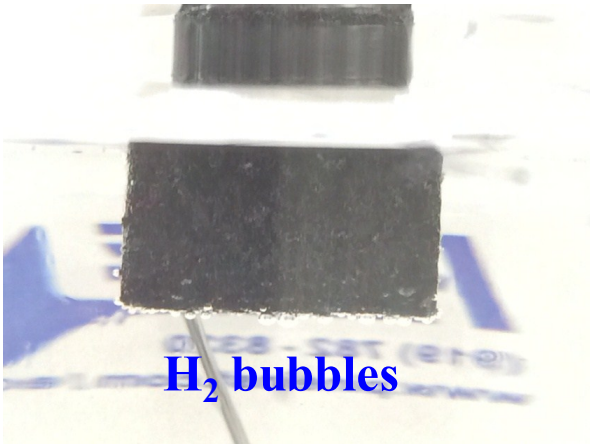

Figure S20. An optical image of EG/$Co_{0.85}Se$/NiFe-LDH electrode during HER reaction; the bubbles indicate the formation of H_2 gas on EG/$Co_{0.85}Se$/NiFe-LDH electrode.

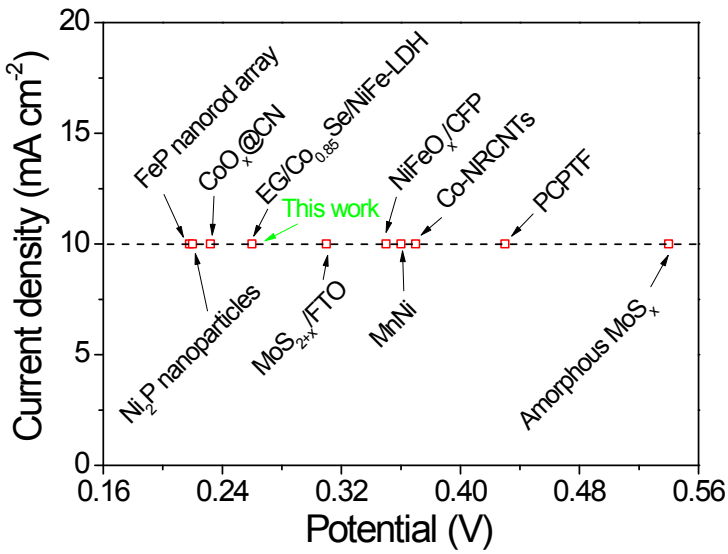

Figure S21. The HER current density at 10 mA cm^{-2} versus overpotential for various catalysts in basic solution.[17]

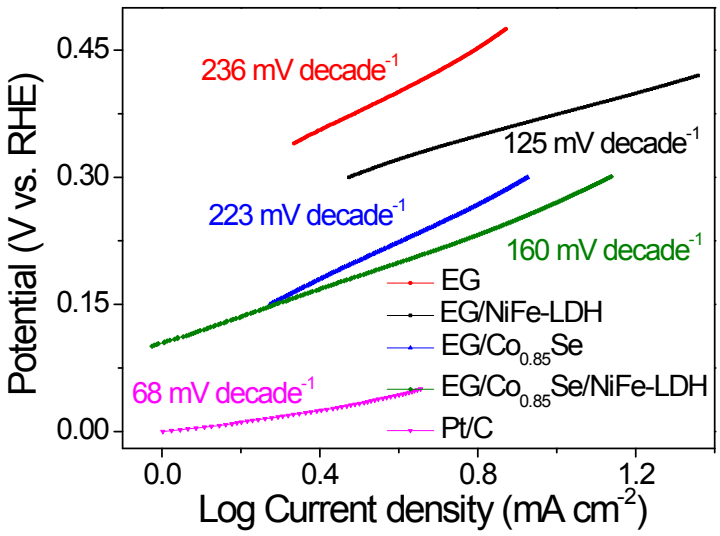

Figure S22. The corresponding Tafel plots from **Figure 4a**.

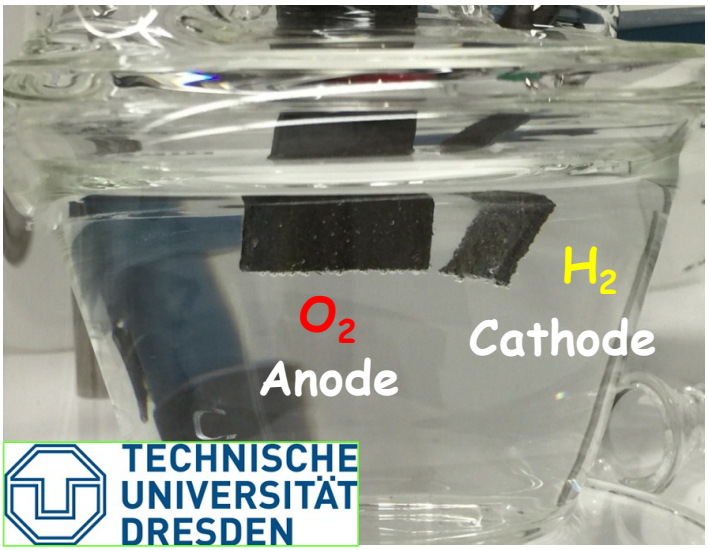

Figure S23. Optical photograph showing the generation of hydrogen and oxygen bubbles from overall water splitting on EG/$Co_{0.85}$Se/NiFe-LDH electrodes in a two-electrode configuration.

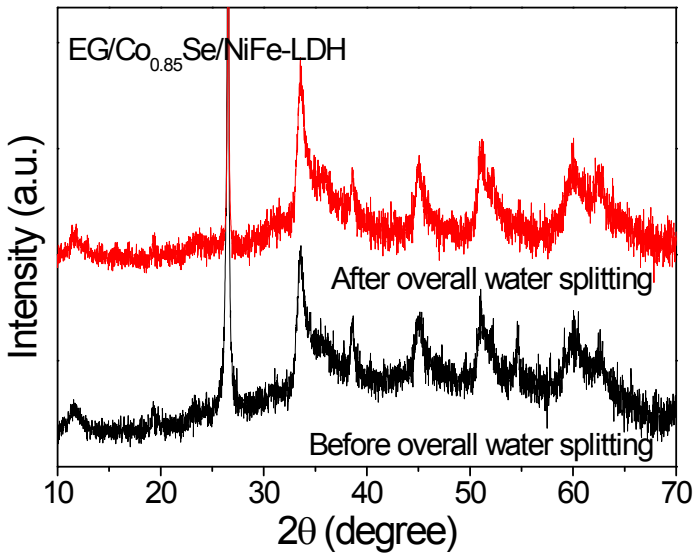

Figure S24. XRD patterns of EG/$Co_{0.85}$Se/NiFe-LDH before and after overall water splitting.

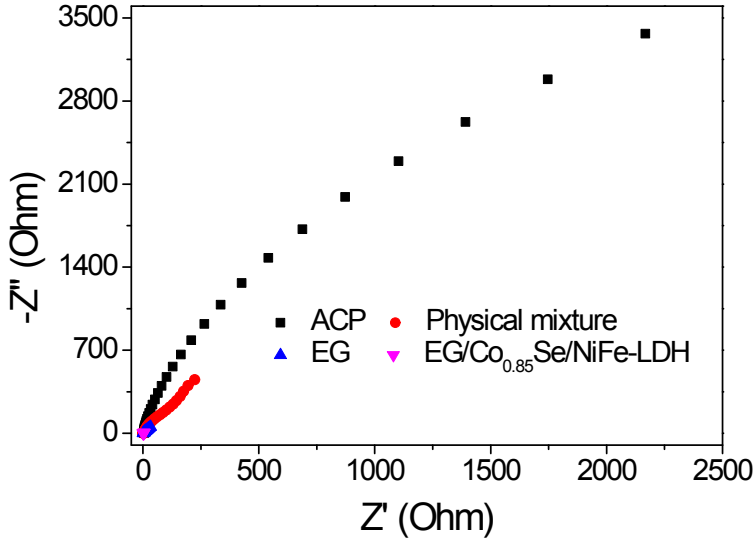

Figure S25. EIS Nyquist plots of ACP, EG, physical mixture of EG, $Co_{0.85}Se$, and NiFe-LDH, and EG/$Co_{0.85}Se$/NiFe-LDH.

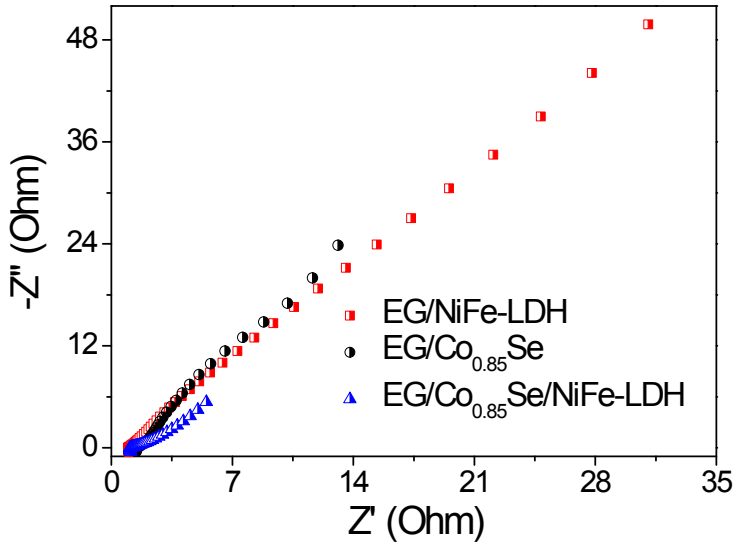

Figure S26. EIS Nyquist plots of EG/$Co_{0.85}Se$, EG/NiFe-LDH, and EG/$Co_{0.85}Se$/NiFe-LDH.

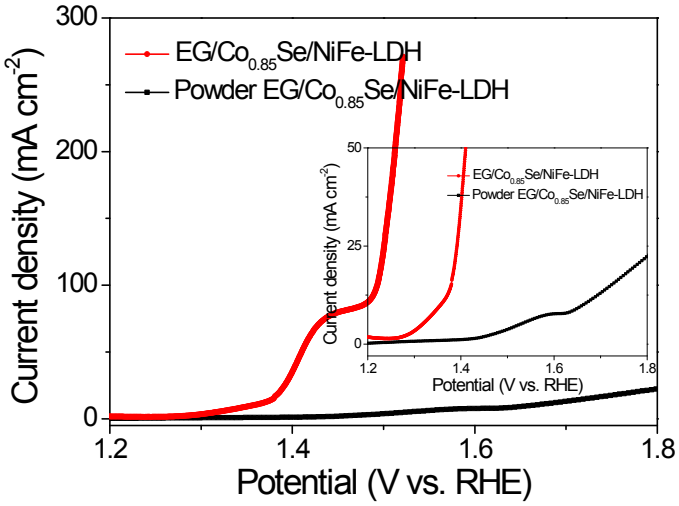

Figure S27. Polarization curves of the EG/$Co_{0.85}$Se/NiFe-LDH and powder EG/$Co_{0.85}$Se/NiFe-LDH obtained by scratching down the EG/$Co_{0.85}$Se/NiFe-LDH from graphite foil and then deposited on glassy carbon electrode in 1.0 M KOH solution.

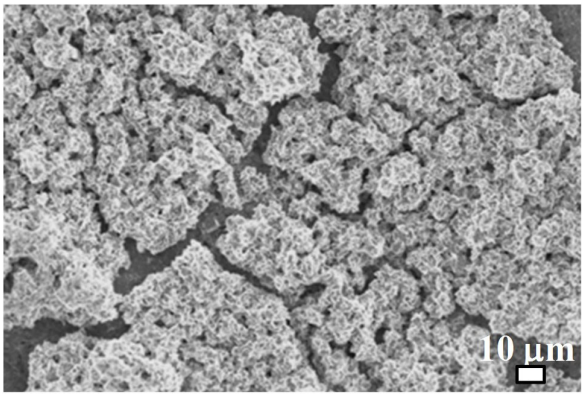

Figure S28. (a) FESEM image of free 3D aggregates of $Co_{0.85}$Se nanosheets without EG as substrates during the synthesis.

Table S1. Comparison of the BET specific surface area of different inorganic nanoarray electrodes.

Author	Catalyst	S_{BET} ($m^2\ g^{-1}$)
This work	**EG/$Co_{0.85}$Se/NiFe-LDH Nanosheets Array**	**156**
Xiaoming Sun[18]	Hierarchical $ZnxCo_{3-x}O_4$ Nanoarrays	78.5
Yiying Wu[19]	$Ni_xCo_{3-x}O_4$ Nanowire Arrays	88
Xuping Sun[20]	CoP Nanowire Arrays	36.5
Xin Wang[21]	FeP Nanowire Arrays	95
Xiongwen Lou[22]	Co_3O_4 Nanosheet Arrays/Ni Foam	118
Xiaoyang Liu[23]	$CoMoO_4$@MnO_2 Core–Shell Nanosheet Arrays	75.8
Tianmo Liu[24]	$NiCo_2S_4$ Nanosheet Arrays	36
Wenjun Zhang[25]	$NiCo_2S_4$ Nanosheet Array	109
Xuping Sun[26]	NiO Nanosheet Array	107
This work	**EG/$Co_{0.85}$Se**	**65**
This work	**EG/NiFe-LDH**	**73**
This work	**EG**	**15**

Table S2. Comparison of OER performance of EG/$Co_{0.85}Se$/NiFe-LDH with some representative non-precious metal OER electrocatalysts.

Author	Catalyst (Loading density (mg cm^{-2}))[a]	Current density (J)	Potential at the corresponding J	Electrolyte
This work	**EG/$Co_{0.85}Se$/NiFe-LDH (4.0 mg cm^{-2})**	**150 mA cm^{-2}**	**1.50 V**	**1 M KOH**
This work	**EG/$Co_{0.85}Se$/NiFe-LDH (4.0 mg cm^{-2})**	**250 mA cm^{-2}**	**1.51 V**	**1 M KOH**
Angew. Chem. Int. Ed. 2015, 54, 6251	Co-P film (2.6 mg cm^{-2})	150 mA cm^{-2}	~ 1.65 V	1 M KOH
Angew. Chem. Int. Ed. 2015, 54, 9351	NiSe/NF (2.8 mg cm^{-2})	150 mA cm^{-2}	~ 1.57 V	1 M KOH
Nat. Commun. 2015, 6, 7261	2-cycle $NiFeO_x$/CFP (1.6 mg cm^{-2})	150 mA cm^{-2}	~ 1.51 V	1 M KOH
Adv. Mater. 2015, 27, 3175	PCPTF (0.1 mg cm^{-2})	30 mA cm^{-2}	~ 1.57 V	1 M KOH
J. Am. Chem. Soc. 2013, 135, 8452	NiFe-LDH/CNT/CFP (0.25 mg cm^{-2})	40 mA cm^{-2}	1.50 V	1 M KOH
Angew. Chem. Int. Ed. 2015, 54,7399	NiCo-r (0.285 mg cm^{-2})	150 mA cm^{-2}	~ 1.69 V	1 M KOH
Nat. Mater. 2011, 10, 780	Co_3O_4/N-rmGO (1.0 mg cm^{-2})	72 mA cm^{-2}	1.60 V	1 M KOH
Chem. Sci. 2014, 5,	Porous Co_3O_4	150 mA cm^{-2}	~ 1.81 V	1 M KOH

3976	atomically-thin sheets (0.34 mg cm^{-2})			
Chem. Sci. 2015, 6, 6624-6631	NiFe-LDH nanoplatelet arrays/Ni foam (1.0 mg cm^{-2})	150 mA cm^{-2}	~ 1.68 V	1 M KOH
Angew. Chem. Int. Ed. 2015, 54, 8722	CoOOH nanosheets (0.15 mg cm^{-2})	50 mA cm^{-2}	~ 1.57 V	1 M KOH
J. Am. Chem. Soc. 2015, 137, 4119	Ni_3N nanosheets (0.285 mg cm^{-2})	150 mA cm^{-2}	~ 1.64 V	1 M KOH
J. Am. Chem. Soc. 2015, 137, 5590	Co_3O_4/$NiCo_2O_4$ DSNCs (1.0 mg cm^{-2})	132 mA cm^{-2}	~ 1.76 V	1 M KOH
Angew. Chem. Int. Ed. 2015, 54, 12004-12008	Single-unit-cell thick $CoSe_2$ sheets (0.17 mg cm^{-2})	70 mA cm^{-2}	~ 1.70 V	1 M KOH
Nano Lett. 2015, 15, 1421	NiCo LDH (0.17 mg cm^{-2})	50 mA cm^{-2}	~ 1.66 V	1 M KOH
Energy Environ. Sci. 2014, 7, 609	N-CG–CoO (0.714 mg cm^{-2})	80 mA cm^{-2}	~ 1.72 V	1 M KOH
ACS Cent. Sci. 2015, 1, 244	ECT-CoNiFeO (---)	150 mA cm^{-2}	~ 1.52 V	1 M KOH
Energy Environ. Sci. 2015, 8, 2347	Ni_2P nanoparticles (0.14 mg cm^{-2})	20 mA cm^{-2}	~ 1.54 V	1 M KOH

Nat. Commun. 2014, 5, 4477	NiFe-NS (0.07 mg cm^{-2})	25 mA cm^{-2}	~ 1.55 V	1 M KOH

[a] A high mass-loading is of great significance for high catalytic performance and real application.[27]

Table S3. Comparison of overall water-splitting performance of EG/$Co_{0.85}Se$/NiFe-LDH with some representative non-precious metal bifunctional electrocatalysts and precious metal (Ir/C and Pt/C) electrocatalysts.

Author	Catalyst (Loading density (mg cm^{-2}))	Current density (J)	Potential at the corresponding J	Electrolyte
This work	**EG/$Co_{0.85}Se$/NiFe-LDH (4.0 mg cm^{-2})**	**10 mA cm^{-2}**	**1.67 V**	**1 M KOH**
This work	**EG/$Co_{0.85}Se$/NiFe-LDH (4.0 mg cm^{-2})**	**20 mA cm^{-2}**	**1.71 V**	**1 M KOH**
Angew. Chem. Int. Ed. 2015, 54, 12361-12365	Ni_5P_4 (~ 3.5 mg cm^{-2})	10 mA cm^{-2}	1.70 V	1 M KOH
Science 2014, 345, 1593-1596	NiFe-LDH (----)	10 mA cm^{-2}	~ 1.70 V	1 M NaOH
Chem. Mater. 2015, 27, 5702-5711	$Ni(OH)_2/NiSe_2$ (0.46 mg cm^{-2})	10 mA cm^{-2}	1.78 V	1 M KOH
Angew. Chem. Int. Ed. 2015, 54, 9351-9355	NiSe/Ni (2.8 mg cm^{-2})	10 mA cm^{-2}	~ 1.63 V	1 M KOH
Angew. Chem. Int. Ed. 2015, 54, 9351-9355	NiSe/Ni (2.8 mg cm^{-2})	20 mA cm^{-2}	1.75 V	1 M KOH
Energy Environ. Sci. 2015, 8, 2347-2351	Ni_2P/NiO_x (0.14 mg cm^{-2})	10 mA cm^{-2}	~ 1.63 V	1 M KOH
Energy Environ. Sci.	Ni_2P/NiO_x	20 mA cm^{-2}	1.70 V	1 M KOH

2015, 8, 2347-2351	(0.14 mg cm^{-2})			
Nat. Commun. 2015, 6, 7261	2-cycle $NiFeO_x$/CFP (3.0 mg cm^{-2})	20 mA cm^{-2}	~ 1.60 V	1 M KOH
J. Am. Chem. Soc. 2015, 137, 14023-14026	Ni_3S_2/Ni (1.6 mg cm^{-2})	13 mA cm^{-2}	1.76 V	1 M NaOH
Nanoscale, 2015, 7, 15122-15126	$NiCo_2S_4$ nanowires array (4.0 mg cm^{-2})	20 mA cm^{-2}	1.85 V	1 M KOH
Nanoscale, 2015, 7, 15122-15126	$NiCo_2O_4$ nanowires array (4.0 mg cm^{-2})	20 mA cm^{-2}	＞ 1.90 V	1 M KOH
This work	**Ir/C (4.0 mg cm^{-2})**	**10 mA cm^{-2}**	**＞ 1.90 V**	**1 M KOH**
This work	**Pt/C (4.0 mg cm^{-2})**	**10 mA cm^{-2}**	**＞ 1.75 V**	**1 M KOH**
This work	**Ir/C (anode)//Pt/C (cathode) (4.0 mg cm^{-2})**	**10 mA cm^{-2}**	**1.62 V**	**1 M KOH**
This work	**Ir/C (anode)//Pt/C (cathode) (4.0 mg cm^{-2})**	**20 mA cm^{-2}**	**1.71 V**	**1 M KOH**

References

[1] K. Parvez, Z.-S. Wu, R. Li, X. Liu, R. Graf, X. Feng, K. Müllen, *Journal of the American Chemical Society* **2014**, *136*, 6083-6091.

[2] J. Duan, S. Chen, B. A. Chambers, G. G. Andersson, S. Z. Qiao, *Advanced Materials* **2015**, *27*, 4234-4241.

[3] S. Chen, J. Duan, J. Ran, M. Jaroniec, S. Z. Qiao, *Energy & Environmental Science* **2013**, *6*, 3693-3699.

[4] Z.-X. Zhang, X.-W. Wang, K.-L. Wu, Y.-X. Yue, M.-L. Zhao, J. Cheng, J. Ming, C.-J. Yu, X.-W. Wei, *New Journal of Chemistry* **2014**, *38*, 6147-6151.

[5] M. Gong, H. Dai, *Nano Res.* **2015**, *8*, 23-39.

[6] C. Xia, Q. Jiang, C. Zhao, M. N. Hedhili, H. N. Alshareef, *Advanced Materials* **2015**, n/a-n/a.

[7] aC.-C. Liu, J.-M. Song, J.-F. Zhao, H.-J. Li, H.-S. Qian, H.-L. Niu, C.-J. Mao, S.-Y. Zhang, Y.-H. Shen, *Applied Catalysis B: Environmental* **2012**, *119–120*, 139-145; bC. Tang, H.-S. Wang, H.-F. Wang, Q. Zhang, G.-L. Tian, J.-Q. Nie, F. Wei, *Advanced Materials* **2015**, *27*, 4516-4522.

[8] A. I. Carim, F. H. Saadi, M. P. Soriaga, N. S. Lewis, *Journal of Materials Chemistry A* **2014**, *2*, 13835-13839.

[9] M. W. Louie, A. T. Bell, *Journal of the American Chemical Society* **2013**, *135*, 12329-12337.

[10] aR. Wu, D. P. Wang, X. Rui, B. Liu, K. Zhou, A. W. K. Law, Q. Yan, J. Wei, Z. Chen, *Advanced Materials* **2015**, *27*, 3038-3044; bY. Hou, T. Huang, Z. Wen, S. Mao, S. Cui, J. Chen, *Advanced Energy Materials* **2014**, *4*, n/a-n/a.

[11] aY. Hou, Z. Wen, S. Cui, S. Ci, S. Mao, J. Chen, *Advanced Functional Materials* **2015**, *25*, 872-882; bY. Hou, F. Zuo, Q. Ma, C. Wang, L. Bartels, P. Feng, *The Journal of Physical Chemistry C* **2012**, *116*, 20132-20139.

[12] Z. Lu, W. Xu, W. Zhu, Q. Yang, X. Lei, J. Liu, Y. Li, X. Sun, X. Duan, *Chemical Communications* **2014**, *50*, 6479-6482.

[13] Z. Li, M. Shao, H. An, Z. Wang, S. Xu, M. Wei, D. G. Evans, X. Duan, *Chemical Science* **2015**.

[14] Z. Wang, Q. Sha, F. Zhang, J. Pu, W. Zhang, *CrystEngComm* **2013**, *15*, 5928-5934.

[15] Z.-H. Sheng, L. Shao, J.-J. Chen, W.-J. Bao, F.-B. Wang, X.-H. Xia, *ACS Nano* **2011**, *5*, 4350-4358.

[16] M. Gong, Y. Li, H. Wang, Y. Liang, J. Z. Wu, J. Zhou, J. Wang, T. Regier, F. Wei, H. Dai, *Journal of the American Chemical Society* **2013**, *135*, 8452-8455.

[17] aY. Yang, H. Fei, G. Ruan, J. M. Tour, *Advanced Materials* **2015**, *27*, 3175-3180; bX. Zou, X. Huang, A. Goswami, R. Silva, B. R. Sathe, E. Mikmeková, T. Asefa, *Angewandte Chemie* **2014**, *126*, 4461-4465; cH. Wang, H.-W. Lee, Y. Deng, Z. Lu, P.-C. Hsu, Y. Liu, D. Lin, Y. Cui, *Nat Commun* **2015**, *6*; dH. Jin, J. Wang, D. Su, Z. Wei, Z. Pang, Y. Wang, *Journal of the American Chemical Society* **2015**, *137*, 2688-2694; eY. Liang, Q. Liu, A. M. Asiri, X. Sun, Y. Luo, *ACS Catalysis* **2014**, *4*, 4065-4069; fC. G. Morales-Guio, L. Liardet, M. T. Mayer, S. D. Tilley, M. Grätzel, X. Hu, *Angewandte Chemie* **2015**, *127*, 674-677; gM. Ledendecker, G. Clavel, M. Antonietti, M. Shalom, *Advanced Functional Materials* **2015**, *25*, 393-399; hD. Merki, S. Fierro, H. Vrubel, X. Hu, *Chemical Science* **2011**, *2*, 1262; iL. Feng, H. Vrubel, M. Bensimon, X. Hu, *Physical Chemistry Chemical Physics* **2014**, *16*, 5917-5921.

[18] X. Liu, Z. Chang, L. Luo, T. Xu, X. Lei, J. Liu, X. Sun, *Chemistry of Materials* **2014**, *26*, 1889-1895.

[19] Y. Li, P. Hasin, Y. Wu, *Advanced Materials* **2010**, *22*, 1926-1929.

[20] J. Tian, Q. Liu, A. M. Asiri, X. Sun, *Journal of the American Chemical Society* **2014**, *136*, 7587-7590.

[21] Y. Yan, L. Thia, B. Y. Xia, X. Ge, Z. Liu, A. Fisher, X. Wang, *Advanced Science* **2015**, *2*, n/a-n/a.

[22] C. Yuan, L. Yang, L. Hou, L. Shen, X. Zhang, X. W. Lou, *Energy & Environmental Science* **2012**, *5*, 7883-7887.

[23] Z. Zhang, F. Bao, Y. Zhang, L. Feng, Y. Ji, H. Zhang, Q. Sun, S. Feng, X. Zhao, X. Liu, *Journal of Power Sources* **2015**, *296*, 162-168.

[24] L. Lin, J. Liu, T. Liu, J. Hao, K. Ji, R. Sun, W. Zeng, Z. Wang, *Journal of*

Materials Chemistry A **2015**, *3*, 17652-17658.

[25] R. Zou, Z. Zhang, M. F. Yuen, M. Sun, J. Hu, C.-S. Lee, W. Zhang, *NPG Asia Mater* **2015**, *7*, e195.

[26] N. Cheng, Q. Liu, J. Tian, X. Sun, Y. He, S. Zhai, A. M. Asiri, *International Journal of Hydrogen Energy* **2015**, *40*, 9866-9871.

[27] aD.-Y. Wang, M. Gong, H.-L. Chou, C.-J. Pan, H.-A. Chen, Y. Wu, M.-C. Lin, M. Guan, J. Yang, C.-W. Chen, Y.-L. Wang, B.-J. Hwang, C.-C. Chen, H. Dai, *Journal of the American Chemical Society* **2015**, *137*, 1587-1592; bY.-R. Zheng, M.-R. Gao, Z.-Y. Yu, Q. Gao, H.-L. Gao, S.-H. Yu, *Chemical Science* **2015**, *6*, 4594-4598; cJ. Tian, Q. Liu, N. Cheng, A. M. Asiri, X. Sun, *Angewandte Chemie International Edition* **2014**, *53*, 9577-9581.